PNAS
www.pnas.org

# Supplementary Information for

## Optical Properties of Metasurfaces infiltrated with Liquid Crystals

**A. Lininger[1] , A. Y. Zhu[1], J. S. Park, G. Palermo, S. Chatterjee, J. Boyd, F. Capasso[2,3] and G. Strangi[2,3]**

**[3] Corresponding Authors. E-mail: capasso@seas.harvard.edu, giuseppe.strangi@case.edu**

**This PDF file includes:**

Supplementary text
Figs. S1 to S5
Legends for Movies S1 to S3
SI References

**Other supplementary materials for this manuscript include the following:**

Movies S1 to S3

www.pnas.org/cgi/doi/10.1073/pnas.2006336117

## Supporting Information Text

## Model for Wetting of Metalens Surface

We present the outlines of a theoretical model for wetting of the metalens, which was referenced in the main text as a means to predict the liquid crystal infiltration behavior. This model,(1, 2) has been used generally to predict the wetting behavior of liquids introduced to nanopatterned pillar arrays (3) beyond the traditional Cassie-Baxter (4) and Wenzel states.(5)

**Simplifications.** In applying this model we have made several assumptions which are not reflective of the experimental metalens infiltration system, but greatly simplify the infiltration equations. The metalens array geometry is in fact a complex spatial distribution of slightly tapered (about 2.8 deg sidewall angle) nanoscale pillars. The geometry furthermore consists of densely packed concentric rings of these nanopillars, alternating with large flat rings of open area. This can lead to complex infiltration behavior which is difficult to predict on the global scale. This behavior is reflected in the observed infiltration dynamics. For simplicity we have ignored these effects and modeled the metalens as an array of nanopillars with globally regular spacing and pillar geometry. We believe this approximation is justified as we are essentially just modeling the densely packed pillared region. Furthermore in this analysis we treat the liquid crystals as an isotropic infiltrating liquid, neglecting long range order. This approximation is reasonable when considering infiltration on the order of the nanopillar spacing.

**Infiltration Equations.** A detailed derivation of these equations can be found in Chen *et al.*, (3) here we will sketch a general outline. Infiltration of the metalens is motivated by the tendency to minimize free energy in the vapor-liquid-substrate (metalens) interfaces after introducing a droplet of the wetting fluid. Variational free energy for the system is calculated as the difference in interficial free energy $\gamma_{xy}$ corresponding to a change in the interface area during infiltration, subject to the condition that the liquid volume remain constant. To minimize this, the infiltrating film can modulate the interficial area by infiltrating from the bulk droplet and either increasing the infiltration in a planar direction, increasing the infiltrated film height $h_f$, or increasing volume in the bulk droplet by refusing further infiltration of the metalens structure. Thus we can calculate the optimal infiltration of the metalens as the energetic equilibrium infiltration state pursuant with the condition of free energy minimization.

Here we consider a regular array of flat topped nanopillars at constant size and spacing. In this case the variational free energy associated with infiltration in the orthogonal planar and vertical directions, respectively, are given by:

$$\mu_x = \frac{\gamma_{lv}[(P^2 - \pi R^2) - cos(\theta_y)(P^2 - \pi R^2 + 2\pi R h_f)]}{h_f(P^2 - \pi R^2)}, \quad [1]$$

$$\mu_z = \frac{\gamma_{lv}[-2\pi R cos(\theta_y)]}{P^2 - \pi R^2}, \quad [2]$$

for $h_f < H$, and:

$$\mu_x = \frac{\gamma_{lv}[P^2 - cos(\theta_y)(P^2 + 2\pi R H)]}{H(P^2 - \pi R^2) + P^2(h_f - H)}, \quad [3]$$

$$\mu_z = 0, \quad [4]$$

for $h_f > H$. Variational free energy corresponding to increasing volume in the bulk droplet is given by

$$\mu_b = \frac{2\pi\gamma_{lv}}{3V_b^{1/3}}\left[\frac{2}{1+cos(\theta^*)} - \frac{S_{sl}cos(\theta_y)}{S_p}\right]\left[\frac{3sin^3(\theta^*)}{\pi(1-cos\theta^*)^2(2+cos\theta^*)}\right]^{2/3}, \quad [5]$$

where P, R and H define the pillar spacing, pillar radius and height of the nanopillar array,respectively, $h_f$ is the film height, $S_{sl}$ and $S_p$ are the interfacial liquid contact area and projected cell area, and $\theta^*$ and $\theta_y$ are the apparent and equilibrium Young's contact angles. As always, Young's contact angle quantifies the intrinsic physical interaction of nonreactive liquids with a solid surface and enters into all equations describing the wetting of liquids on real solid surfaces by encoding the interficial free energies:

$$cos(\theta_y) = \frac{\gamma_{sv} - \gamma_{ls}}{\gamma_{lv}} \quad [6]$$

**Theoretical Infiltration.** We have characterized the metalens infiltration system properties through a measurement of the apparent and equilibrium contact angles using a contact angle goniometer. Details can be seen in Fig. S1. Measurements of the substrate geometrical array parameters were obtained from Scanning Electron Microscopy (SEM) images of the metalens surface and were used to define the dense array. The infiltration was characterized by calculating the variational free energy associated with each proposed direction of infiltration, and choosing the direction of infiltration which corresponds to a minimization in the variational free energy. The system was then stepped forward a small amount in this direction and the variational free energies were recalculated. This was continued until the system reached an equilibrium state or the simulation domain was fully infiltrated. In this way the system approaches an overall minimum in the interfacial free energy, which we expect to correspond with the experimental state of the system.

## Methods

**Infiltration Procedure.** The liquid crystal is first introduced to the metalens by a small droplet of liquid crystal which is pipetted onto the center of the metalens surface. The droplet is pulled into the lens through the wetting properties of the nanostructure composing the metalens, and this wetting process is described within the manuscript. The droplet is then lightly blown into the metalens surface from directly above with compressed air, to aid in the spreading of the droplet. Once the wetting front has been observed to have progressed throughout the entire structure, any excess from the droplet is removed from the surface by blowing at an angle with the compressed air. Another droplet is placed in contact with the side of the metalens to act as a reservoir for liquid to be drawn in and out of the system. Finally the infiltrated system is allowed to rest for 24 hours to stabilize the infiltrate height.

**Focal Spot PSF Measurement.** The point spread function (PSF) of the metalens at the focal point is measured with a custom-built microscope consisting of a collimated laser source (Cobalt 06-MLD diode laser, 633 $nm$, $< 1.2\,nm$ bandwidth), neutral density filters for incidence intensity control, beam expander optics, objective (50x, NA=0.5, 566036, *Leica*), tube lens ($f = 200\,mm$, LA1708, *Thorlabs*), and a commercial CMOS camera (BFS-U3-200S6M-C,*FLIR*), see Fig. S4. The objective, tube lens, and CMOS array are mounted on a z-axis linear translator for PSF measurements along the optic axis. The 1 cm diameter metalens is illuminated with total intensity of 5 mW as measured through an aperture of the same size.

**Z-axis Intensity Distribution Measurement.** The objective is first placed on the focal plane of the metalens to obtain its focal spot image. The imaging optics, consisting of an objective, a tube lens, and a CMOS camera, is then translated along the optical axis toward and away from the metalens, while capturing the PSF image at every $50 \pm 10\,\mu m$, for $400\,\mu m$ in each direction. From each captured PSF image, the FWHM of the central peak is obtained. The obtained central peak's FWHM information is then stacked to represent the intensity distribution along the optic axis near the focus.

**Infiltration Height Measurement.** A tilting compensator (B 0-5 Lambda, *Leica*) was used to determine the height of infiltrated nematic liquid crystal thickness within the metalens structure. Under plane-polarized light, progressive rotation of the compensator about its horizontal axis decreases retardation of the rays emerging from the observed NLC filled metalens. The tilting angle was read from a calibrated micrometer drum, which measures a corresponding decrease in retardation. By exploiting the simple relation between the phase retardation ($\Delta\Gamma$), thickness ($t$) and birefringence ($\Delta n$): $\Delta\Gamma = t\Delta n$ we can estimate the thickness of the infiltrated liquid crystal.

The reported accuracy is 2.5 - 8 nm of variation in optical path difference (1OPD). For the measurement of infiltrated liquid crystal height in the metalens, the compensator is first placed at maximum light intensity then rotated in increments corresponding to 0.25 $\mu m$, to identify the distance along the sample experiencing full compensation (dark condition). The measurement was repeated several times in each sections of the metalens after 1 hour and 24 hours from the infiltration, respectively. See Fig. S3. As seen in the thickness map, at 1 hour after infiltration the liquid crystal remains mainly near in the edge of the metalens with an average height of about 2.00 $\mu m$, while the filled level decreases near to the metalens center. The infiltrated liquid crystal thickness changes drastically 24 hours after the infiltration process, resulting in a much more even distribution within the structure, with an average height of about 0.85 $\mu m$. However this distribution of infiltration height is still highly irregular over the entire structure. It is clear that the infiltration process depends strongly on specific infiltration parameters and the amount of liquid crystal available for wetting.

**Optical Simulations.** Simulations were performed with a commercial finite difference time domain solver (Lumerical). The metalens was run at a reduced size (50um diameter, comprising of two zones) while maintaining approximately the same numerical aperture of 0.1 as the actual metasurface lens used in experiments. Perfectly matched layers (PML) were used for all boundaries. The near field at a distance of two lambda (here $\lambda = 633$ nm) away from the metalens was computed, and subsequently far field transform techniques were used to propagate the near field into the far field to obtain the theoretical point spread functions and focal spot profiles. We calculated the equivalent surface currents from the near field data and evaluated the superposition of resulting fields at each point in space, which was performed within Lumerical. From this the point spread functions and focal spot profiles in the far field were obtained.

## References

1. J Bico, U Thiele, D Quéré, Wetting of textured surfaces. *Colloids Surfaces A: Physicochem. Eng. Aspects* **206**, 41 – 46 (2002).
2. J Bico, C Tordeux, D Quéré, Rough wetting. *EPL* **55**, 214 (2001).
3. H Chen, H Zang, X Li, Y Zhao, Toward a better understanding of hemiwicking: A simple model to comprehensive prediction. *Langmuir* **35**, 2854–2864 (2019).
4. A Cassie, S Baxter, Wettability of porous surfaces. *Transactions Faraday Soc.* **40**, 546–550 (1944).
5. RN Wenzel, Resistance of solid surfaces to wetting by water. *Ind. & Eng. Chem.* **28**, 988–994 (1936).

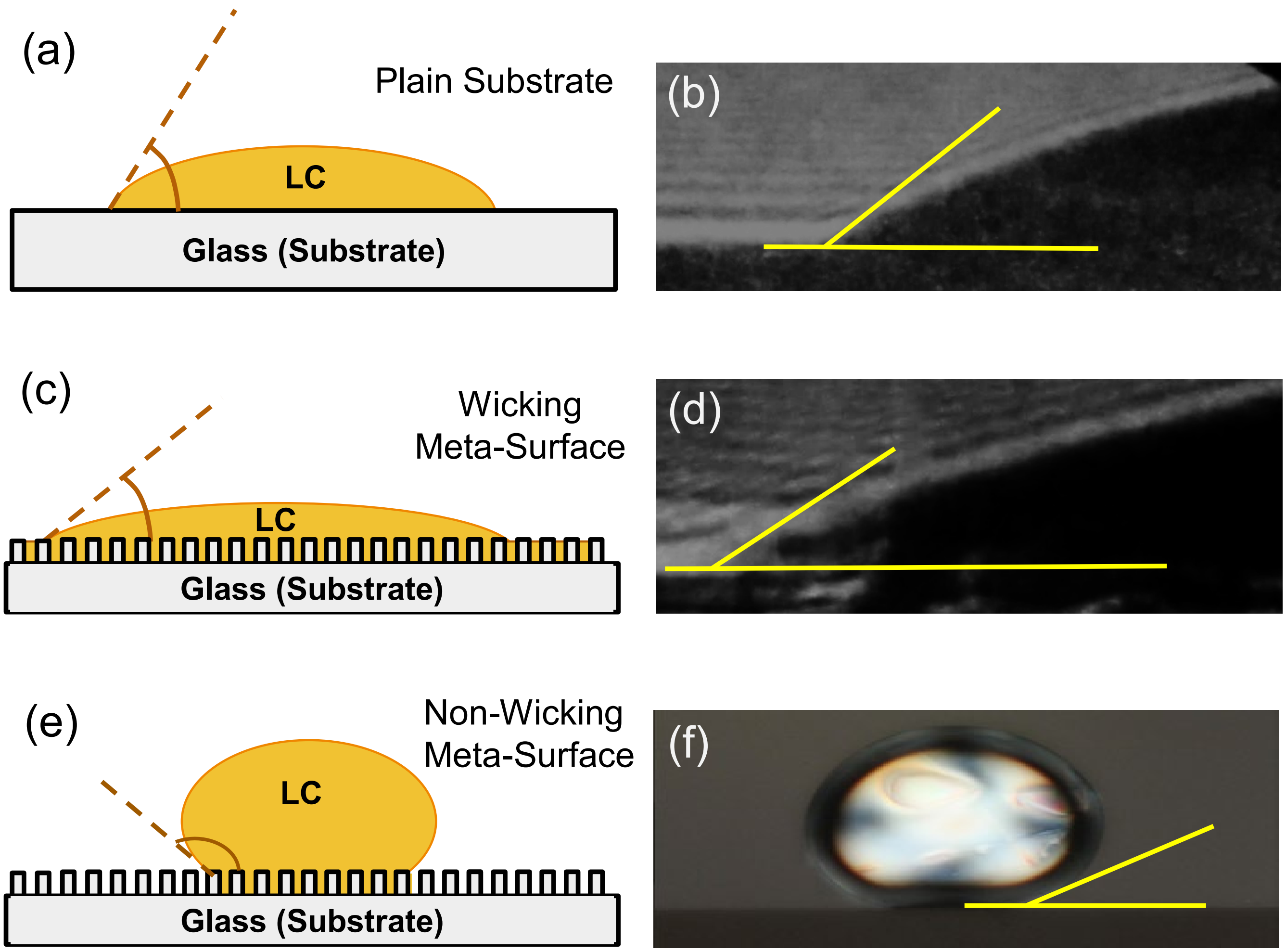


**Fig. S1.** Experimental measurement of liquid-substrate contact angle to determine the wettability of the substrate. Illustration **(A,C,E)** and experimental **(B,D,F)** image of contact angle for liquid crystal E7 droplet on a **(A,B)** plain fused-silica glass substrate, **(C,D)** on the experimental metalens surface, **(E,F)** on a hydrophobic nanopillared substrate which the liquid will not infiltrate. A higher affinity for infiltration causes the droplet to spread out and decrease the apparent contact angle, while a hydrophobic surface does not promote wicking, leading to a higher apparent contact angle.

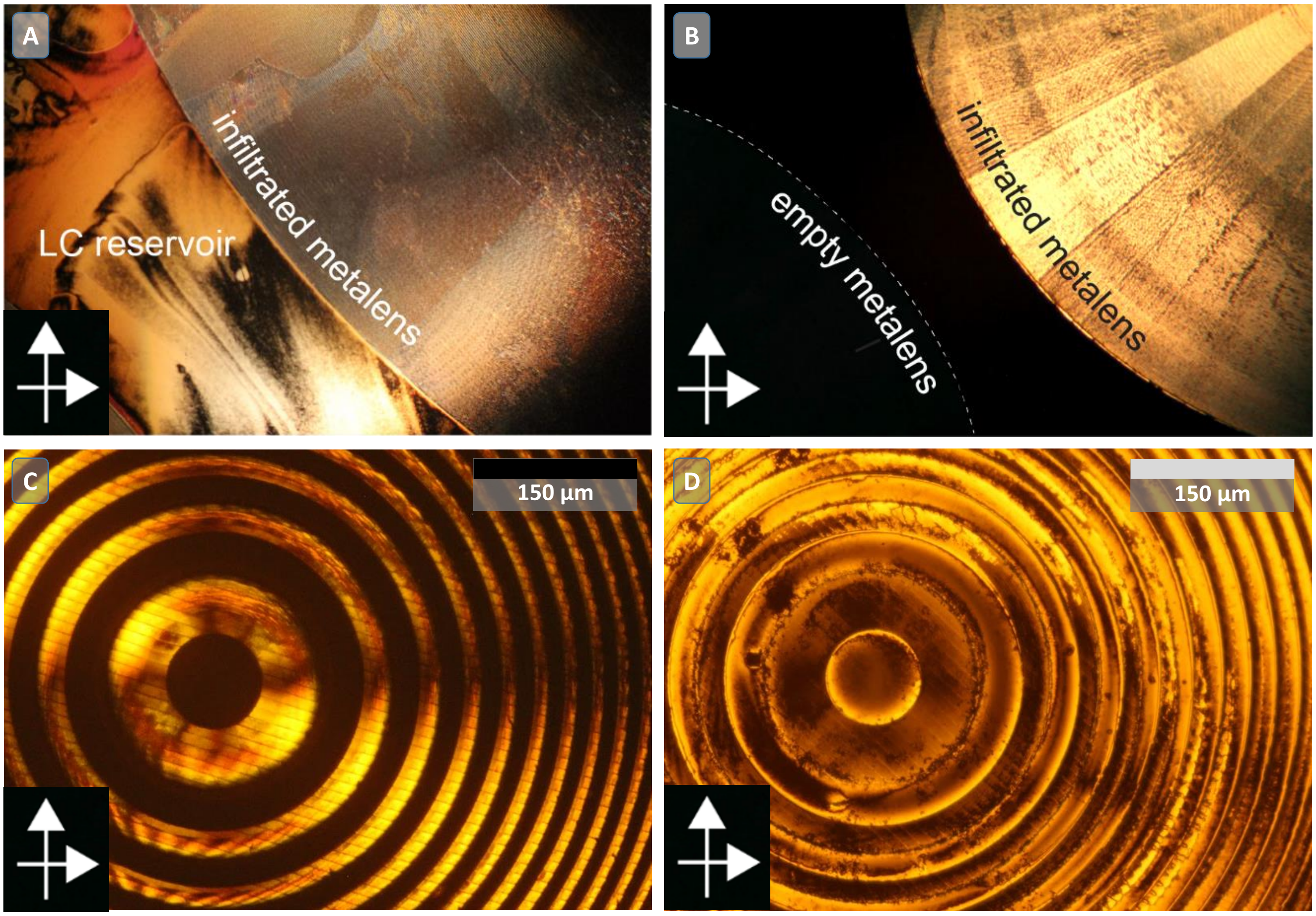


**Fig. S2.** **(A)** Polarized optical microscopy image of nematic liquid crystal (E7) reservoir closed to an infiltrated metalens edge. **(B)** There is a clear difference between an un-infiltrated metalens and a metalens infiltrated with E7. The un-infiltrated lens edge appears dark under crossed polarizers.**(C)** Central portion of the metalens before and **(D)** after E7 liquid crystal infiltration, shown under crossed polarizers.

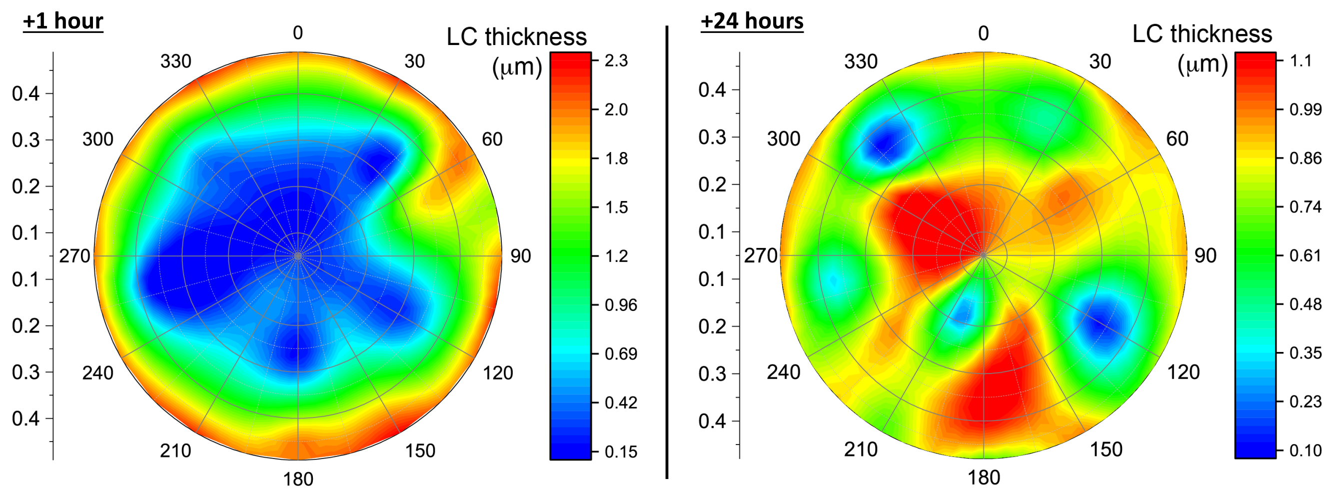


**Fig. S3.** Infiltrated liquid crystal thickness within the metalens structure 1hour (**left**) and 24hours (**right**) after the NLC infiltration procedure. The thickness is not uniform throughout the metalens.

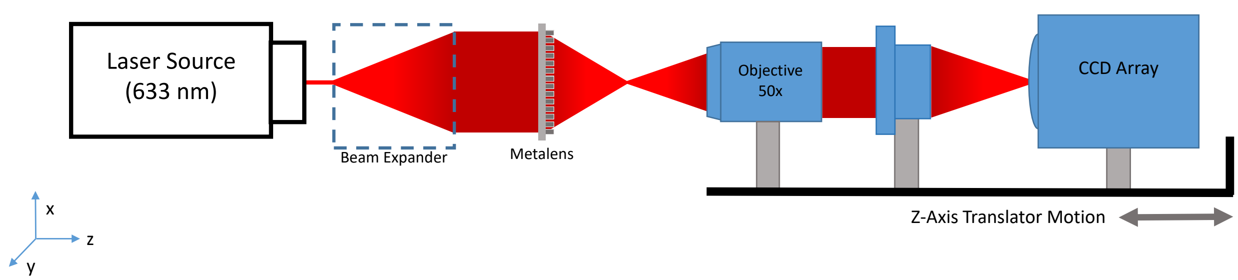


**Fig. S4.** Experimental setup for PSF characterization. The diode laser source (Cobolt 06-MLD) is expanded and collimated with bulk optics, and is then passed through the metalens. An objective (Leica, 50x) collects the image of the metalens' focal point, and a tube lens ($f = 200\ mm$) focuses the collected image to a CMOS camera (FLIR, BFS-U3-200S6M-C). The objective, the tube lens, and the CMOS camera are mounted on a z-axis translator for PSF measurements along the optic axis.

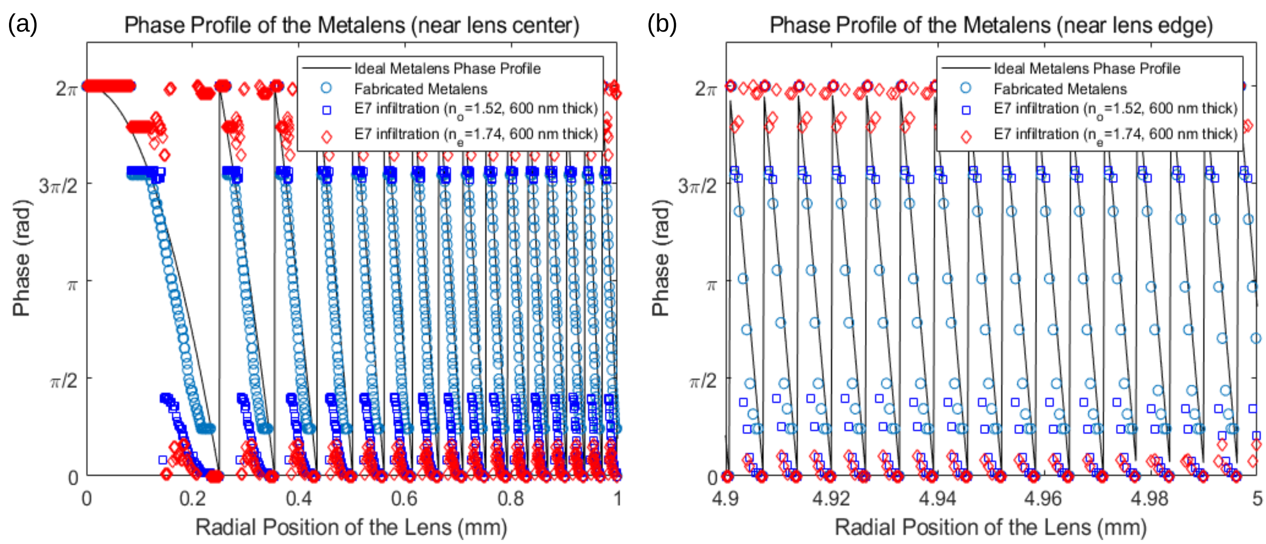


**Fig. S5.** Phase profile of individual elements comprising the metalens before and after infiltration with NLC, at **(A)** the center and **(B)** near the edge of the metalens respectively. The imparted phase from each nanopillar changes significantly due to the presence of the NLC, resulting in a reduced phase gradient which leads to significant spherical aberrations.

**Movie S1. Metalens infiltration with nematic liquid crystal MBBA, shown in parallel polarization and crossed polarization states at x1 playback speed.**

**Movie S2. Metalens infiltration with nematic liquid crystal E7, shown in parallel polarization and crossed polarization states at x1 playback speed.**

**Movie S3. Hologram producing nanostructure infiltration with nematic liquid crystal MBBA, shown in parallel polarization and crossed polarization states at x1 playback speed.**